# Underground Object Characterization based on Neural Networks for Ground Penetrating Radar Data

Yu Zhang, Dryver Huston, Tian Xia

yzhang19@uvm.edu, dhuston@uvm.edu, txia@uvm.edu
School of Engineering, University of Vermont, Burlington, VT 05405

## ABSTRACT

In this paper, an object characterization method based on neural networks is developed for GPR subsurface imaging. Currently, most existing studies demonstrate detecting and imaging objects of cylindrical shapes. While in this paper, no restriction is imposed on the object shape. Three neural network algorithms are exploited to characterize different types of object signatures, including object shape, object material, object size, object depth and subsurface medium's dielectric constant. Feature extraction is performed to characterize the instantaneous amplitude and time delay of the reflection signal from the object. The characterization method is evaluated utilizing the data synthesized with the finite-difference time-domain (FDTD) simulator.

**Keywords:** ground penetrating radar, object detection, pattern recognition, neural networks, non-destructive evaluation.

## 1. INTRODUCTION

Ground penetrating radar (GPR) is the main subsurface imaging tool for non-destructive infrastructure evaluation, such as rebar detection [1], bridge deck inspection [2], soil moisture assessment [3], railroad ballast monitoring [4]-[5], etc. In these non-destructive evaluation (NDE) applications, buried object characterization, including object shape identification, object material classification, object size estimation, object depth detection, is one methodological objective. Currently many researches have been focusing on some aspects, while very few have been demonstrated to deal with all of them. In Ref. [6], mathematic models are developed to simulate the hyperbolic signatures of buried cylindrical objects and calculate the objects sizes. However, as the developed mathematic are specific to certain object shapes, the application scope of this method is limited. Gaussian process (GP) regression [7] is developed to characterize the relationship between a set of extracted features and the object size. The limitation of this method is that it requires to use the material property parameters as the input for GP regression, which are generally unknown for most non-destructive underground inspection. Synthetic aperture radar (SAR) imaging method [8] has been proposed to address the problem of inverse scattering and reconstruction of buried objects, which nevertheless requires the pre-knowledge of the dielectric constant of the burying medium. Therefore, to relax the restrictions, it is valuable to develop a method that can effectively characterize the object shape, material type, size and burying depth as well as the permittivity of the burying medium simultaneously.

Neural networks are a family of tools in machine learning to approximate functions from a large number of inputs. Neural networks are generally presented as systems of interconnected "neurons" which exchange messages among each other. The neurons interconnections have tunable numeric weights, which makes neural nets adaptive to inputs and capable of learning. Neural networks have been utilized in many applications, such as medical decision making [10], hyperspectral image classification [11], traffic sign classification [12], human action recognition [13], and radar detection [14]-[15], etc. Neural network approaches have been developed in some preliminary researches [16]-[17] for GPR buried object characterization, whereas they are restricted to the cylindrical objects whose cross-section are circles. In this paper, an object characterization method based on neural networks regression and classification is proposed and developed, which emphasizes on estimating the shape, material type, size and depth of the buried object as well as the dielectric constant of the underground medium simultaneously.

The rest sections of the paper are organized as followings. Sec. 2 describes feature extraction procedures for object characterization. Sec. 3 introduces the basic architecture of neural networks and proposes the object characterization method. In Sec. 4, the proposed neural network algorithms are trained and evaluated using finite-difference time-domain (FDTD) simulation data sets. Sec. 5 summarizes the concluding remarks.

## 2. FEATURE EXTRACTION FOR OBJECT CHARACTERIZATION

During the GPR inspection, radar antennas have conical beams. As shown in Figure 1, a reflection signal can be received and recorded by the antennas that are not directly above the scattering object. As the GPR antennas receive the reflection signals from the buried object from a number of different angles while with varying wave propagation distance and amplitude, the buried object in GPR B-Scan image show the hyperbolic image feature.

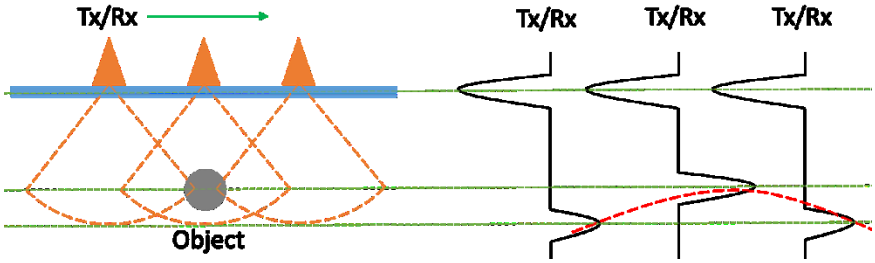


Figure 1. Typical GPR reflection signal from a buried object

For each hyperbola composition point, its time index and signal amplitude are determined by a number of object properties, including the depth, size, material type and object shape and the dielectric constant of burying medium. Therefore, a function can be extracted to characterize the relationship between the amplitude and time index of each point and the buried objects properties. In this paper, A-scan signal amplitude and time index of the reflected pulse are extracted as the input to the neural networks.

### 2.1 Signal envelope extraction

Before extracting the data features, Hilbert Transform is applied to extract the pulse envelope that measures the signal power. The Hilbert Transform of signal $s(t)$ can be considered as the convolution of $s(t)$ with the function $h(t) = \frac{1}{\pi t}$, which can be expressed as

$$\hat{s}(t) = \mathcal{H}\{s\} = h(t) * s(t) = \int_{-\infty}^{\infty} s(\tau)h(t-\tau)d\tau = \frac{1}{\pi}\int_{-\infty}^{\infty} \frac{s(\tau)}{t-\tau} d\tau \quad (1)$$

To eliminate the singularities, such as $\tau = t$ and $\tau = \pm\infty$, Hilbert Transform is defined using the Cauchy principal value. Correspondingly, the Hilbert Transform of $s(t)$ is calculated as

$$\hat{s}(t) = \mathcal{H}\{s\} = -\frac{1}{\pi}\lim_{\varepsilon \downarrow 0} \int_{\varepsilon}^{\infty} \frac{s(t+\tau)-s(t-\tau)}{\tau} d\tau \quad (2)$$

Applying Hilbert transform to GPR signal $s(t)$, the analytic signal is obtained as

$$s_a(t) = s(t) + i\hat{s}(t) \quad (3)$$

where $\hat{s}(t)$ is the direct output of the Hilbert Transform of $s(t)$. The magnitude of $s_a(t)$ equals

$$|s_a(t)| = \sqrt{s(t)^2 + \hat{s}(t)^2} \quad (4)$$

$|s_a(t)|$ is the envelope of $s(t)$, which facilitates the signal power characterization.

Figure 2 demonstrates signal power characterization using Hilbert transform. The waveform on left is a GPR A-Scan waveform produced from two scatters. In the A-Scan waveform, the first pulse is the antennas' direct coupling, while the second and third pulses are the reflection signals from the 1st and 2nd scatters correspondingly. As the transmitting pulse signal is the Ricker wavelet (the second order derivatives of Gaussian function), the backscattering pulse from each object or layer interface shows three peaks. The waveform on right side is produced by the Hilbert transform where the three peaks become much more discernible.

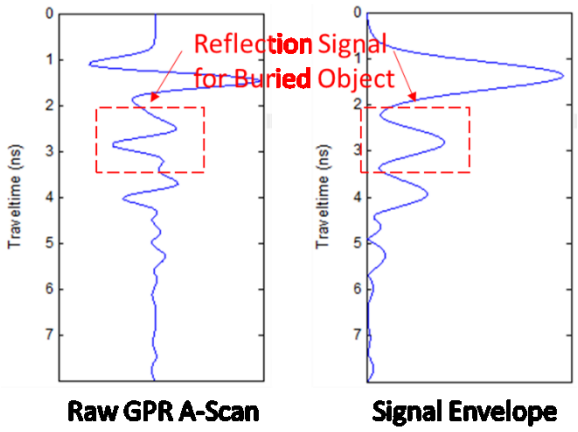


Figure 2. Hilbert transform for signal power characterization

### 2.2 Object feature extraction

The object feature extraction procedures are:

Step 1: Denoting the number of A-Scan trace in the B-Scan image as $N$, initialize two $N \times 1$ vectors: "$Amplitude$" and "$Time$".

Step 2: For the $i$th A-Scan trace $s(t)$ in the B-Scan image, calculate the envelope signal $|s_a(t)|$ using Hilbert transform.

Step 3: Search the maximum amplitude in the envelope signal $|s_a(t)|$. Record the amplitude value as $A_0$ and the corresponding time index as $t_0$.

Step 4: If $s(t_0) < 0$, then assign $Amplitude(i) = -A_0$; else, assign $Amplitude(i) = A_0$.

Step 5: Assign $Time(i) = t_0$.

Repeat Steps 2-5 for all the A-Scan traces.

Finally, both the vectors "$Amplitude$" and "$Time$" are fed to the neural networks as the inputs.

## 3. NEURAL NETWORKS APPROACH

### 3.1 Neural networks

Neural networks are composed of simple elements operating in parallel. These elements are inspired by biological nervous systems. As in nature, the connections between elements largely determine the network function. A neural network can be trained to perform a particular function by adjusting the values of the connections or weights among elements.

To describe neural networks, the definition of the "neuron" is introduced first. The diagram in Figure 3 denotes a single neuron. The neuron is a computational unit that takes inputs $x_1, x_2, \ldots, x_n$ and a bias term $b$ and produces the output:

$$h_{W,b}(x) = \varphi(W^T x) = \varphi(\sum_{i=1}^{n} W_i x_i + b) \tag{5}$$

where $\varphi: \Re \to \Re$ is called the activation function which defines the mapping from inputs to output in a single neuron, and $W_i$ is the weight for the $i$th input $x_i$.

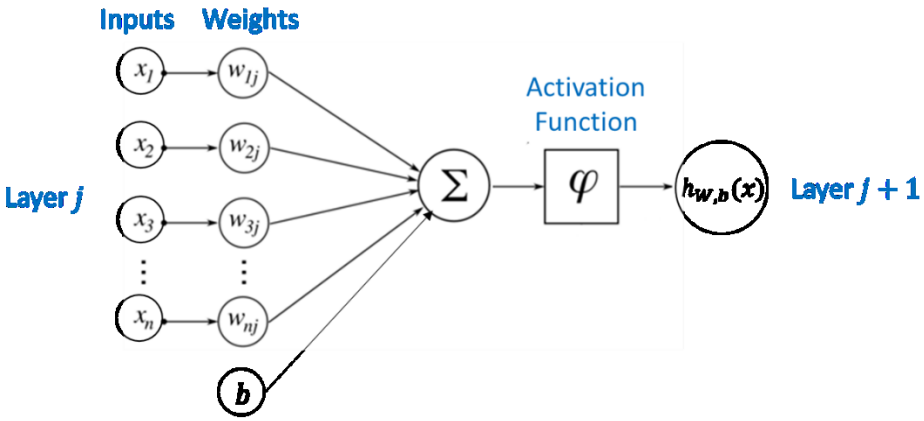


Figure 3. One neuron in Neural Networks

A neural network is constructed by hooking together many neurons, which means the output of a neuron can be the input of another neuron. Figure 4 depicts the architecture of a 3-4-2 neural network. In this neural network, the leftmost layer is the input layer, and the rightmost layer is the output layer. The middle layer of nodes is the hidden layer, because values of each node are not observed in the training set. A neural network can consist of multiple hidden layers. The example neural network has 3 input units, 4 hidden units, and 2 output units.

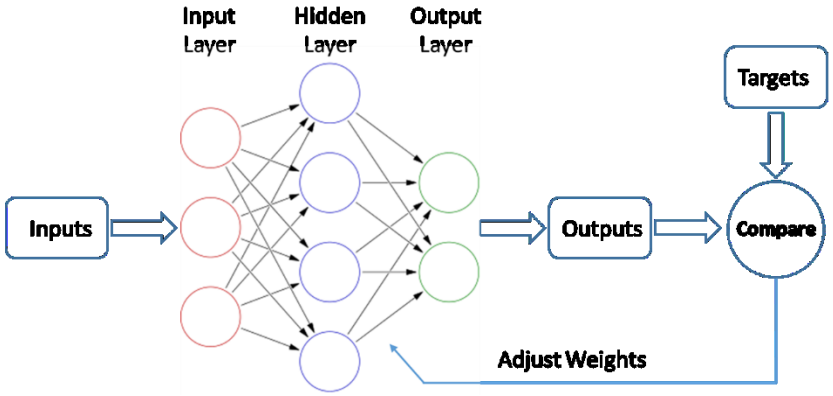


Figure 4. Neural networks architecture

Typically, neural networks are adjusted, or trained, so that a particular input leads to a specific target output. During the training procedure, the input as well as its expected target are fed to the neural network. As shown in Figure 4, the network is adjusted, based on a comparison of the output and the target, until the network output matches the target. Generally, many such input/target pairs are needed to train a neural network. Upon the training, the neural network should be able to produce suitable outputs for any given inputs.

### 3.2 Object characterization method

The flowchart of the proposed buried object characterization method is plotted as Figure 5, where three neural networks are constructed and utilized.

Neural Network 1: For each B-Scan image, 21 A-Scan traces in the middle are selected for feature extraction. Along the hyperbola curve, the composing points' amplitude and time index values are extracted as two $21 \times 1$ verctors $\boldsymbol{A}$ and $\boldsymbol{B}$ respectively to construct a $42 \times 1$ parameter vector $\boldsymbol{I_1} = \begin{bmatrix} \boldsymbol{A} \\ \boldsymbol{B} \end{bmatrix}$, which is fed to the 1st neural network as input. Then the 1st neural network produces the object shape as the result. Denoting the objects are classified into $M$ shapes, the output of the neural network is a $M \times 1$ vector $\boldsymbol{O_1} = [s_1\ s_2\ \cdots\ s_M]^T$, where $s_i = 1$ if the object is determined as the $i$th shape, otherwise, $s_i = 0$.

Neural Network 2: The object shape vector $\boldsymbol{O_1}$ is combined with the $42 \times 1$ feature vector $\boldsymbol{I_1}$ as the new $(42 + M) \times 1$ feature vector $\boldsymbol{I_2} = \begin{bmatrix} \boldsymbol{I_1} \\ \boldsymbol{O_1} \end{bmatrix}$. The updated feature vector is fed to the 2nd neural network as the input. The output of the 2nd neural network is the material type of the object. Denoting the objects are classified into $L$ types of materials, the output of the neural network is a $L \times 1$ vector $\boldsymbol{O_2}$, where the $i$th element is 1 when the object is determined as the $i$th type of material, while other elements are all 0.

Neural Network 3: The input of the 3rd neural network is the combination of the object material and the previous $(42 + M) \times 1$ feature vector which produce a $(42 + M + L) \times 1$ vector $\boldsymbol{I_3} = \begin{bmatrix} \boldsymbol{I_2} \\ \boldsymbol{O_2} \end{bmatrix}$. The outputs of the 3rd neural network are depth and size of the object as well as the dielectric constant of the underground medium, which is a $3 \times 1$ vector $\boldsymbol{O_3}$. The 1st element in $\boldsymbol{O_3}$ is the object depth, the 2nd element is the object size, and the 3rd element is the dielectric constant of the burying medium. In particularly, the value of the object size represents the horizontal spanning width of the buried object.

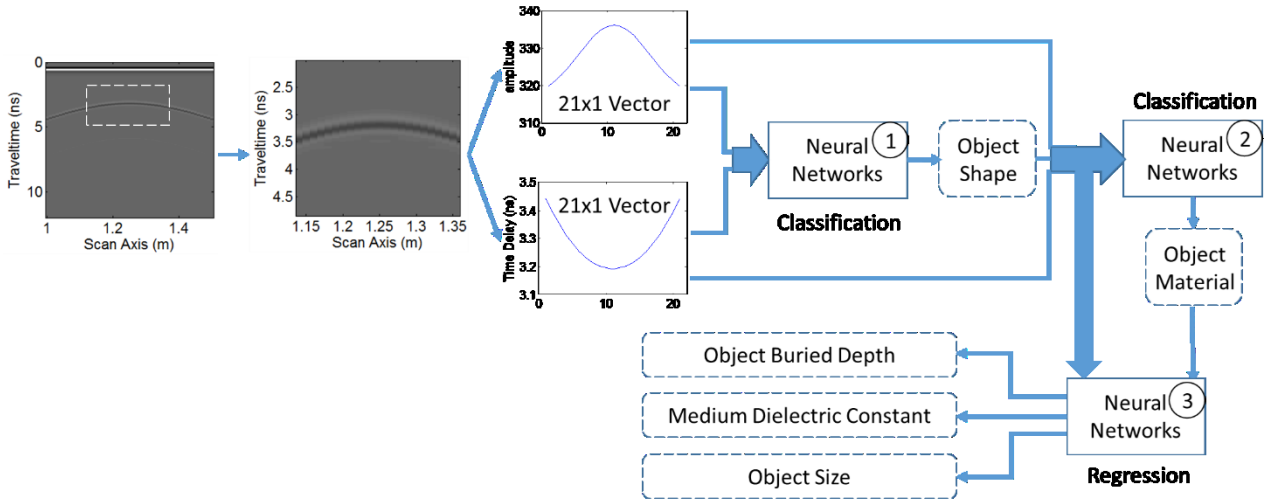


Figure 5. Proposed object characterization method

During the implementation of the neural networks, three sets of data are provided: (1) Training sets are presented to the network during the training procedure, and the network is adaptive adjusted in accordance with the fitting error. (2) Validation data sets are used to measure network generalization, and to halt training when generalization stops improving. (3) Testing data sets are used to provide an independent measure of network performance after training.

For classification purpose, the 1st and 2nd neural networks in the proposed method are implemented as a two-layer feed-forward network respectively. The architecture of such neural networks is displayed as Figure 6. The activation function for the hidden layer is a sigmoid function, and the activation function for the output layer is a softmax function. The network is trained with scaled conjugate gradient backpropagation algorithm [19]. The training procedure automatically stops when generalization stops improving, which is quantitatively evaluated by the cross-entropy error of the validation samples. The 1st neural network in the proposed method contains 42 input units, 20 hidden units and 1 output unit for implementation. The 2nd neural network contains 43 input units, 20 hidden units and 1 output unit for implementation.

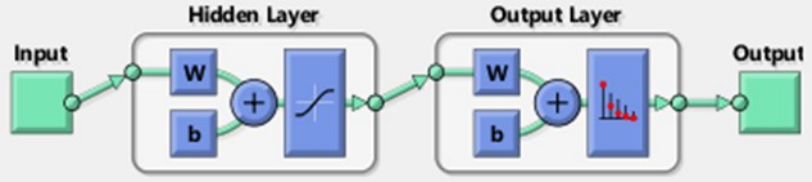


Figure 6. Architecture of neural network for classification

For function regression purpose, the 3rd neural network in the proposed method is implemented as a two-layer feed-forward network whose activation functions for hidden layer and output layer are sigmoid function and linear function

respectively. The architecture of such neural network is plotted as Figure 7. The network is trained with Levenberg-Marquardt backpropagation algorithm [20]. The training procedure automatically stops when generalization stops improving, which is evaluated using the mean square error (MSE) of the validation samples. This neural network contains 44 input units, 40 hidden units and 3 output units.

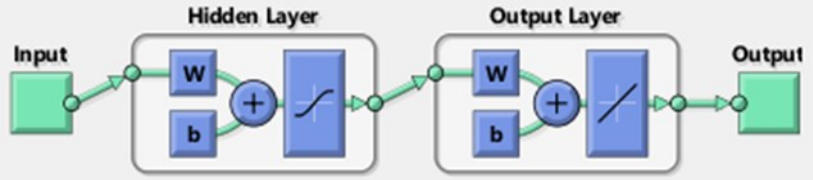


Figure 7. Architecture of neural network for function regression

## 4. EXPERIMENTS ON SIMULATED GPR DATA

### 4.1 Data Set Configuration

In order to evaluate the proposed object characterization method, experiments on GPR inspection data are conducted. The test utilizes the data set synthesized with the FDTD simulation program GprMaxV2.0 [21]. In the FDTD simulation, the GPR waveform is generated as a Ricker waveform (i.e. negative normalized second derivative of a Gaussian pulse) with its center frequency being 2.3 GHz. The sampling frequency is set to 170 GHz and the time window is set as 12 ns. GPR A-Scan traces are collected from left to right along the horizontal direction uniformly at every 1 cm distance. GPR transceiver antennas are located 2.5 mm above the ground surface. The subsurface is modeled as a homogeneous layer of 0.6 m thickness.

Various acquisition scenarios are generated during the FDTD simulation. The characteristics of the buried objects are selected as follows:

(1) Object depth: 0.15 m, 0.20 m, 0.25 m, 0.30 m;

(2) Dielectric constant of underground medium: 4, 6, 8;

(3) Object material type with different dielectric constant values: air ($\varepsilon = 1$), limestone ($\varepsilon = 10$), metal ($\varepsilon = \infty$);

(4) Object size: 5 cm, 10 cm, 15 cm, 20 cm;

(5) Object shape: circle, square, triangle.

Therefore, totally 432 data sets with different geometry configurations are synthesized for neural networks training and testing. In particularly, the value of the object size represents the horizontal dimension of the buried object. The geometry configuration as well as the corresponding B-Scan image for setup: a 10 cm × 10 cm square metal object buried at 0.2 m in the medium with $\varepsilon = 6$ are shown in Figure 8.

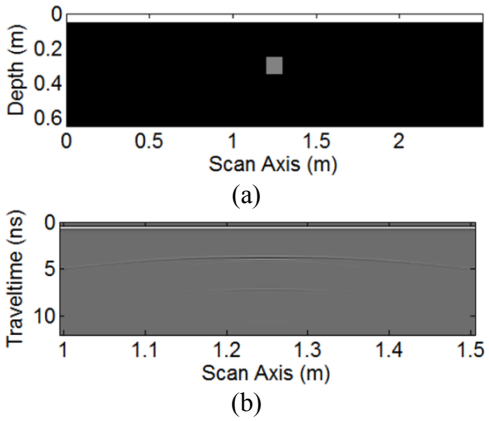


Figure 8. Geometry configuration and B-Scan image example

For each data set, the feature vector is extracted as the input and the geometry ground truth is served as target data for neural networks. The 432 data sets are randomly divided into three groups: training group, validation group, and testing group. During the neural networks implementation, $432 \times 70\% = 302$ data sets are used as training data, $432 \times 15\% = 65$ data sets are used as validation data, and $432 \times 15\% = 65$ data sets are used as testing data.

### 4.2 Experimental Results

The 1st neural network in the proposed method aims to classify the shape of buried object into three categories: circle, square and triangle. The output of the neural network is one of the vectors $[1 \quad 0 \quad 0]^T$, $[0 \quad 1 \quad 0]^T$ or $[0 \quad 0 \quad 1]^T$, which represents the object is circle, square or triangle respectively. The classification result is shown in Table 1. The average classification success rate is 90.0%, while the classification success rate for circle, square and triangle objects are 84.7%, 91.0% and 94.4% respectively. The test results indicate that the proposed object characterization method can successfully identify the shape of buried object based on GPR B-Scan image.

Table 1. Success rate of object shape classification

| | Circle | Square | Triangle | Average |
|---|---|---|---|---|
| Classification Success (%) | 84.7 | 91.0 | 94.4 | 90.0 |

Upon the object shape recognition, the 2nd neural network in the proposed method is designed to divide the material of buried object into three types: air, limestone and metal. The classification results are summarized in Table 2. The success rates for both the square and triangle objects are both 100%. The only classification error happens when the neural network tried to recognize a metal circular object. The classification results demonstrate that the proposed object characterization method performs very well for distinguishing the material types of buried objects.

Table 2. Success rate of object material type classification

| Classification Success (%) | Air | Limestone | Metal |
|---|---|---|---|
| Circle Objects | 100.0 | 100.0 | 97.9 |
| Square Objects | 100.0 | 100.0 | 100 |
| Triangle Objects | 100.0 | 100.0 | 100 |
| All Objects | 100.0 | 100.0 | 99.3 |

Upon the object shape and material identification, the 3rd neural network in the proposed method is developed to estimate the object depth, object size and dielectric constant of the burying medium. To quantitatively evaluate the estimation performance, the average relative error is calculated for each object feature and summarized in Table 3. For the object depth, the estimation error is 3.93%, while for the medium dielectric constant, the estimation error is 5.51%. The test results indicate that the proposed method can accurately estimate the depth of the object and the dielectric constant of the burying medium.

Table 3. Object characterization performance

| Average Relative Error (%) | Object Depth | Medium Dielectric Constant | Object Size |
|---|---|---|---|
| Circle Objects | 2.14 | 4.51 | 9.91 |
| Square Objects | 4.87 | 9.03 | 8.05 |
| Triangle Objects | 4.80 | 3.00 | 29.55 |
| All Objects | 3.93 | 5.51 | 15.83 |

For the object size estimation, the relative error is 15.83%, which is mainly degraded by the triangle object test cases. The calculation results show that the proposed method can successfully estimate the object size for circular and square

objects. While for triangle object size estimation, the proposed method needs further improvements. A larger training data sets should be generated and the better selection for input GPR B-Scan image feature vector should be discussed in further work.

## 5. CONCLUSIONS

In this paper, the possibility of underground object characterization based on neural networks for GPR inspection [22] data is investigated. An object characterization method consisting of three neural network algorithms are proposed to identify the shape and material of the buried object as well as estimate the depth and size of the object. Experiments on FDTD simulated data demonstrates that the performance of the proposed method is promising.

## REFERENCE


[1] Venkatachalam, A.S., Xu, X., Huston, D. and Xia, T., "Development of a New High Speed Dual-Channel Impulse Ground Penetrating Radar," IEEE Journal of Selected Topics in Applied Earth Observations and Remote Sensing 7(3), 753-760 (2014).

[2] Zhang, Y., Candra, P., Wang, G. and Xia, T., "2-D Entropy and Short-Time Fourier Transform to Leverage GPR Data Analysis Efficiency," IEEE Transactions on Instrumentation and Measurement 64(1), 103-111 (2015).

[3] Zhang, Y., Burns, D., Huston, D. and Xia, T., "Sand moisture assessment using instantaneous phase information in ground penetrating radar data," Proc. SPIE 9437, 943726 (2015).

[4] Zhang, Y., Venkatachalam, A.S., Xia, T., Xie, Y., and Wang, G., "Data analysis technique to leverage ground penetrating radar ballast inspection performance," 2014 IEEE Radar Conference, 463-468 (2014).

[5] Zhang, Y., Venkatachalam, A.S. and Xia, T., "Ground-penetrating radar railroad ballast inspection with an unsupervised algorithm to boost the region of interest detection efficiency," Journal of Applied Remote Sensing 9(1), 1-19 (2015).

[6] Chang, C.W., Lin, C.H., and Lien, H.S., "Measurement radius of reinforcing steel bar in concrete using digital image GPR," Construction and Building Materials 23(2), 1057-1063 (2009).

[7] Pasolli, E., Melgani, F. and Donelli, M., "Gaussian Process Approach to Buried Object Size Estimation in GPR Images," IEEE Geoscience and Remote Sensing Letters 7(1), 141-145 (2010).

[8] Zhang, Y. and Xia, T., "OFDM and compressive sensing based GPR imaging using SAR focusing algorithm," Proc. SPIE 9437, 943725 (2015).

[9] Hagan, M.T., Demuth, H.B., Beale, M.H. and Jesus, O.D., [Neural Network Design (2nd Edition)], Martin Hagan (2014).

[10] Mazurowski, M.A., Habas, P.A., Zurada, J.M., Lo, J.Y., Baker, J.A. and Tourassi, G.D., "Training neural network classifiers for medical decision making: The effects of imbalanced datasets on classification performance," Neural Networks 21(2-3), 427-436 (2008).

[11] Ratle, F., Camps-Valls, G. and Weston, J., "Semisupervised Neural Networks for Efficient Hyperspectral Image Classification," IEEE Transactions on Geoscience and Remote Sensing 48(5), 2271-2282 (2010).

[12] Ciresan, D., Meier, U., Masci, J. and Schmidhuber, J., "Multi-column deep neural network for traffic sign classification," Neural Networks 32, 333-338 (2012).

[13] Ji, S., Xu, W., Yang, M. and Yu, K., "3D Convolutional Neural Networks for Human Action Recognition," IEEE Transactions on Pattern Analysis and Machine Intelligence 35(1), 221-231 (2013).

[14] Leung, H., Dubash, N. and Xie, N., "Detection of Small Objects in Clutter Using a GA-RBF Neural Network," IEEE Transactions on Aerospace and Electronic Systems 38(1), 98-118 (2002).

[15] Gong, M., Zhao, J., Liu, J., Miao, Q. and Jiao, L., "Change Detection in Synthetic Aperture Radar Images Based on Deep Neural Networks," IEEE Transactions on Neural Networks and Learning Systems 27(1), 125-138 (2016).

[16] Caorsi, S. and Cevini, G., "An Electromagnetic Approach Based on Neural Networks for the GPR Investigation of Buried Cylinders," IEEE Geoscience and Remote Sensing Letters 2(1), 3-7 (2005).

[17] Bermani, E., Caorsi, S. and Raffetto, M., "Microwave Detection and Dielectric Characterization of Cylindrical Objects From Amplitude-Only Data by Means of Neural Networks," IEEE Transactions on Antennas and Propagation 50(9), 1309-1314 (2002).

[18] Zhang, Y., Venkatachalam, A.S., Huston, D. and Xia, T., "Advanced signal processing method for ground penetrating radar feature detection and enhancement," Proc. SPIE 9063, 906318 (2014).

[19] Moller, M.F., "A scaled conjugate gradient algorithm for fast supervised learning," Neural Networks 6(4), 525-533 (1993).

[20] Hagan, M.T., and Menhaj, M., "Training feed-forward networks with the Marquardt algorithm," IEEE Transactions on Neural Networks 5(6), 989–993(1994).

[21] Giannopoulos, A., "Modeling ground penetrating radar by GprMax," Construction and Building Materials 19(10), 755-762 (2005).

[22] Xia, T., Xu, X.L.,Venkatachalam, A. and Huston, D. "Development of a High Speed UWB GPR for Rebar Detection," *Proceedings of IEEE International Conference on Ground Penetrating Radar (2012).*